Numerical simulation of high drag reduction in a turbulent channel flow with polymer additives

By Yves Dubief

1. Introduction

The addition of small amounts of long chain polymer molecules to wall-bounded flows can lead to dramatic drag reduction. Although this phenomenon has been known for about fifty years, the action of the polymers and its effect on turbulent structures are still unclear. Detailed experiments have characterized two distinct regimes (Warholic *et al.* 1999), which are referred to as low drag reduction (LDR) and high drag reduction (HDR). The first regime exhibits similar statistical trends as Newtonian flow: the log-law region of the mean velocity profile remains parallel to that of the Newtonian flow but its lower bound moves away from the wall and the upward shift of the log-region is a function of drag reduction, DR. Although streamwise fluctuations are increased and transverse ones are reduced, the shape of the rms velocity profiles is not qualitatively modified. At higher drag reductions, of the order of 40-50%, the flow enters the HDR regime for which the slope of the log-law is dramatically augmented and the Reynolds shear stress is small (Warholic *et al.* 1999; Ptasinski *et al.* 2001). The drag reduction is eventually bounded by a maximum drag reduction (MDR) (Virk & Mickley 1970) which is a function of the Reynolds number. While several experiments report mean velocity profiles very close to the empirical profile of Virk & Mickley (1970) for MDR conditions, the observations regarding the structure of turbulence can differ significantly. For instance, Warholic *et al.* (1999) measured a near-zero Reynolds shear stress, whereas a recent experiment (Ptasinski *et al.* 2001) shows evidence of non-negligible Reynolds stress in their MDR flow. To the knowledge of the authors, only the LDR regime has been documented in numerical simulations (Sureshkumar *et al.* 1997; Dimitropoulos *et al.* 1998; Min *et al.* 2001; Dubief & Lele 2001; Sibilla & Baron 2002). This paper discusses the simulation of polymer drag reduced channel flow at HDR using the FENE-P (Finite Elastic non-linear extensibility-Peterlin) model which was used for the first LDR simulation by Sureshkumar *et al.* (1997). Flow and polymer parameters are close to realistic polymer drag reducing conditions. High drag reductions are achieved by using finite differences and a robust time stepping technique. A minimal channel flow is also used as a numerical experiment to investigate the effect of the outer region turbulent structures on the overall drag at HDR. The drag reducing action of the model is finally studied through the structure of energy transfers from the polymers to the velocity components. This investigation sheds some light on the details of polymer drag reduction.

2. Governing equations and numerical method

The formalism of the constitutive equations for viscoelastic flows typically includes the assumption of uniform concentration of the polymer solution, and the momentum

equations thus become:

$$\partial_t u_i = -u_j\partial_j u_i - \partial_i p + \frac{\beta}{Re}\partial_j\partial_j u_i + \underbrace{\frac{1-\beta}{Re}\partial_j \tau_{ij}}_{f_i} , \tag{2.1}$$

where β is the ratio of the solvent viscosity ν to the total viscosity and effectively controls the concentration of polymers. The Reynolds number is defined as $Re = Uh/\nu$, where the velocity, U, and length, h, scale are defined in the next section. Note the addition of the viscoelastic stress which is later referred to as f_i. The viscoelastic tensor τ_{ij} in f_i is obtained by solving the FENE-P equation,

$$\boldsymbol{\tau} : \partial_t c_{ij} = -\underbrace{u_k\partial_k c_{ij}}_{\text{advection}} + \underbrace{c_{kj}\partial_k u_i + c_{ik}\partial_k u_j}_{\text{stretching}} - \underbrace{\frac{1}{We}\left(\frac{c_{ij}}{1-\frac{c_{kk}}{L^2}} - \delta_{ij}\right)}_{=\tau_{ij}:\text{relaxation}} + \kappa D(c_{ij}) , \tag{2.2}$$

where the conformation tensor, c_{ij}, is the phase average of $q_i q_j$, q_i being the component of the end-to-end vector of each individual polymer which has a maximum dimensionless extensibility, L. The Weissenberg number We is the ratio of the largest polymer relaxation time λ to the flow time scales, such that $We = \lambda U/h$. The numerical method is essentially that of Min *et al.* (2001) modified to simulate very elastic and long polymer molecules. The successful modification, consisting of a novel time advancement scheme for Eq. (2.2), is described and validated in Dubief *et al.* (2003). In the present paper only a brief outline of the method is given. The momentum equations are solved on a staggered grid with second-order central finite differences. The divergence of the polymer stress (Eq. 2.1) and the spatial derivatives of c_{ij} are computed using a fourth order compact scheme and a third order upwind compact scheme, respectively. Time advancement of Eqs. (2.1) and (2.2) is performed by the classical semi-implicit second-order Crank-Nicolson/third-order Runge-Kutta scheme. In the momentum equation, the Newtonian viscous stress are treated implicitly in the wall-normal direction. Eq. (2.2) is solved with a new semi-implicit time scheme which guarantees the trace of the c_{ij} remains upper bounded ($c_{kk} < L^2$).

In turbulent flows, Eq. (2.2) proves to be fairly stiff and therefore delicate to solve. Originally, Sureshkumar *et al.* (1997) added a diffusive term to the FENE-P ($D(c_{ij}) = \partial_k\partial_k c_{ij}$) and used a fairly significant diffusivity coefficient κ. Min *et al.* (2001) later pointed out that the addition of a diffusivity everywhere in the flow causes the smearing of polymer stress gradients and suggested a local approach. The Local Artificial Dissipation (LAD) is a second-order numerical error ($D(c_{ij}) = \Delta_k^2\partial_k^2 c_{ij}$, Δ_k denoting the local grid size) which is applied only to nodes for which the positiveness of the conformation tensor is not satisfied. Min *et al.* designed the LAD as an-extra diffusion of the scheme used for the advection of c_{ij}.

As discussed in Dubief *et al.* (2003), the advection term in Eq. (2.2) creates small scales similar to the ones observed for a passive scalar at high-Schmidt number, *i.e.* a few orders of magnitude smaller than the dissipative flow scale, the Kolmogorov scale. The LAD allows the polymer field to develop sharper gradients than a global diffusivity approach, however the quality of the simulation depends strongly on the resolution of the smallest turbulent scales. When the drag is very close to its Newtonian value, direct numerical simulations can only resolved up to Kolmogorov which is then the cutoff scale for the advection of c_{ij}. At HDR, the turbulence is so reduced that the simulation of

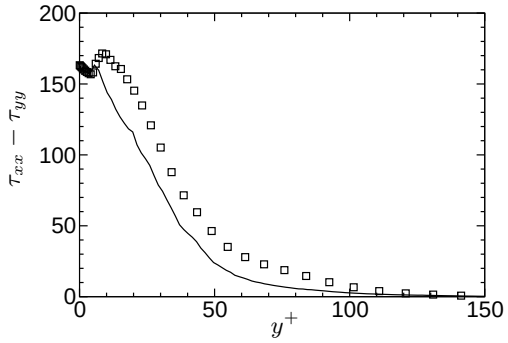

FIGURE 1. *Left*: Normal stress profiles of the viscoelastic simulation L100W120MC, □ , compared to the Brownian dynamic simulation ,——— .

smaller scales for the conformation tensor becomes possible. The quality of a FENE-P simulation is assessed by comparing the polymer stress obtained by Eq. (2.2) and the one obtained with a Brownian dynamic simulation (Terrapon *et al.* 2003). Since the Brownian simulation is only a one-way coupling from the flow to polymers, the comparison is achieved by using the velocity field computed from the viscoelastic simulation. In the case of HDR (Fig. 1) the agreement is within 10% which is considered satisfactory.

Finally, as in any simulation involving dramatic reduction of drag, particular attention to the dimensions of the computational domain must be paid. Here, simulations are performed in a channel flow, where periodicity is enforced in the homogeneous direction, x and z, and no-slip is prescribed on the walls. Periodicity is a very satisfactory boundary condition providing that the energy-containing turbulent structures are smaller than the dimensions of the computational domain. In the case of polymer drag reduction, a coarsening of the streaks is observed (White *et al.* 2003), suggesting that all turbulent scales in the near-wall region are likely to grow with increasing drag reduction. As demonstrated by Jiménez & Moin (1991) in their numerical experiment of the minimal flow unit capable of sustaining turbulence, turbulence vanishes when the computational domain is smaller than 1000 by 100 wall units in the streamwise and spanwise directions, respectively. The wall unit is defined the ratio of the kinematic viscosity ν to the friction velocity $u_\tau = \sqrt{\nu(dU/dy)_{wall}}$. Based on the Newtonian friction velocity, the length and width of the computational domain have been varied from 1000 to 6000 and from 300 to 1200, respectively for a drag reduction of $DR = 60\%$. While velocity correlations in the streamwise direction do not go exactly to zero, even for $L_x^+ = 6000$, the difference in drag reduction is less than 1% for a domain 4000×1200 compared with 6000×1200. In the spanwise direction, correlations drop to zero for $L_z^+ = 1200$, which has led us to choose the intermediate domain $4000 \times 600 \times 1200$ or $4\pi h \times 2h \times 4h$ in integral units, as shown in Table 1. In the course of the study of the channel dimensions, it was noticed that turbulence never disappears in the smallest domain, in spite of its sub-critical dimension in drag reduction mode with $L_x^+ \simeq 600$ and $L_z^+ \simeq 150$ (based on the reduced skin-friction). Results obtained with this domain are also discussed as a numerical experiment.

Simulations are performed in a channel flow at an intermediate Reynolds number, $Re = 7500$ based on the half-width h of the channel and the centerline velocity of the initial Poiseuille profile. The bulk Reynolds number is $Re_M = 5000$. Conservation of the mass flow is imposed which gives $h^+ = hu_\tau/\nu = 300$. The resolution is $\Delta x^+ = 9$, $\Delta y^+ = 0.1-5$ and $\Delta z^+ = 6$, when normalized by the skin friction at $DR = 0\%$. Statistics

Name	Line/symbol	Dimensions	L	$We_{\tau 0}$	β	DR
L60W84LC	●	$4\pi h \times 2h \times 4h$	60	84	0.9	47%
L60W84MC	○	$\pi h \times 2h \times h$	60	84	0.9	67%
L100W120LC	■	$4\pi h \times 2h \times 4h$	100	120	0.9	60%
L100W120MC	□	$\pi h \times 2h \times h$	100	120	0.9	72%

TABLE 1. Polymer parameters used for the viscoelastic simulations. The Weissenberg number $We_{\tau 0}$ is normalized the wall-shear stress for the Newtonian simulation ($DR = 0\%$). For clarity, data from simulation L60W84MC appear only on the mean velocity profile plot (Fig 2).

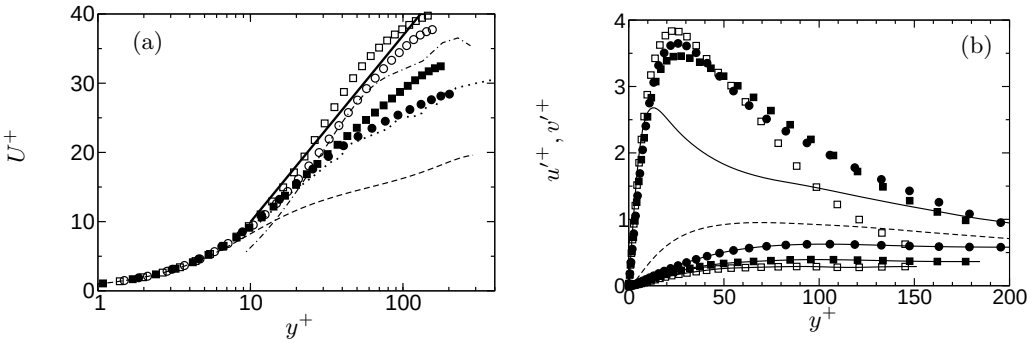

FIGURE 2. *Left*: Mean velocity profiles scaled with inner variables. – – – – : Newtonian simulation ($DR = 0\%$); ——— : MDR asymptote, $U^+ = 11.7 \ln y^+ + 17$. Experimental data (White *et al.* 2003): ····· , $DR = 45\%$; —·— , $DR = 67\%$. Other symbols and lines are defined in Table 1. *Right*: RMS of velocity fluctuations scaled with inner variables. Newtonian simulation ($DR = 0\%$): ——— , u'^+; – – – – , v'^+. For the viscoelastic simulations, symbols are defined in Table 1, u'^+ is denoted by symbols only; v'^+ is indicated by symbols connected by ——— .

are collected over 300 to 400 convection times h/U, starting after the transient period, typically $200h/U$.

3. Results

In the following, the simulations are referred as to by LxxWyyCD, where xx, yy and CD designate respectively the dimensionless maximum extensibility L, yy the Weissenberg number normalized the Newtonian wall-shear and CD the computational domain, MC for minimal channel, LC for large channel (see Table 1).

Two observations can readily be made from table 1. First the FENE-P model requires fairly high Weissenberg numbers to achieve HDR with long-chain type polymers, while HDR has experimentally been measured for We ranging from unity to 100. The need for high We can be attributed to the underestimation of polymer stress by the model in the case of low extension, and therefore be blamed on the simplicity of the FENE-P model, based on a dumbbell, neglecting internal modes. The second observation arises from the comparison between drag reductions obtained with the minimal channel and the larger domain. For $L = 60$ and $We_\tau 0 = 84$, the difference is the largest, with the minimal channel showing 20% more reduction than the large domain. As discussed in the previous section, turbulence in the minimal channel flow under condition of drag reduction is very likely to be affected by the periodic boundary conditions. In the present case, the streamwise turbulent intensity is significantly reduced around the centerline (Fig. 2b),

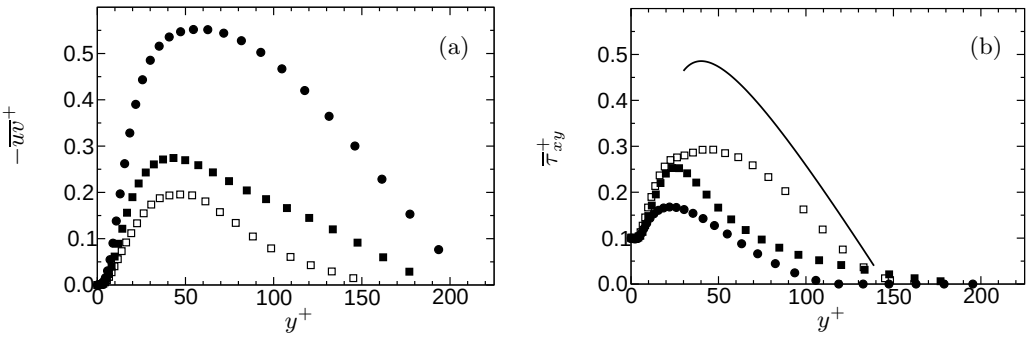

FIGURE 3. Reynolds shear stress (3a) and polymer stress (3b) normalized by u_τ and ν. Symbols are defined in Table 1. In Fig. 3b, ——— represents the contribution the polymer stress would have to Eq. (3.1) in the case of MDR defined by the velocity profile $U^+ = 11.7\ln(y^+) - 17$ and $-\overline{uv}^+ = 0$.

indicating that large scale turbulent structures which are otherwise present in the large domain cannot develop. Deprived of this energy coming from the outer region of the flow, the near-wall region produces a weaker shear.

All the mean velocity profiles domain exhibit a change of slope in the log-law region, but only the ones obtained with minimal channel flow approach Virk's asymptote, shown by a solid line in Fig. 2a. For L60W84LC ($DR = 47\%$), the slope of the log region is roughly twice that of the Newtonian, which ascertains the fact that this simulation belongs to the lower part of the HDR regime, while L100W120LC is intermediate. In the case of the minimal channel, increasing We for this simulation had no effect on the amount of drag reduction. The simulation L100W120MC seems thus representative of an asymptotic state for the constraints imposed by the boundary condition channel flow. Also plotted in Fig. 2a are some experimental data obtained at Stanford by White *et al.* (2003), showing that similar results velocity profiles can be obtained in a turbulent boundary layer with non-uniform polymer concentration.

The turbulent velocity fluctuations (Fig. 2b) behave as observed experimentally (see White *et al.* 2003). The peak of u' shifts away from the wall and its magnitude increases slowly compared to the Newtonian flow when normalized by u_τ. The wall-normal component v' follows an opposite trend; w' behaves as v' and consequently does not appear on the plot for clarity. In drag reduced flow, the maximum of ${u'}^+$ is indeed higher or comparable with the $DR = 0\%$ case, as found in experiments (Warholic *et al.* 1999; Ptasinski *et al.* 2001; White *et al.* 2003). The strong reduction of the transverse fluctuations suggests that polymers target preferentially the vortices, which have a significant contribution to the transverse velocity components.

The balance of stresses,

$$-\overline{uv}^+ - \left(1 - \frac{y^+}{h^+}\right) + \beta\frac{dU^+}{dy^+} + (1-\beta)\overline{\tau}^+_{xy} = 0\,, \tag{3.1}$$

contains significant information regarding the mechanism of polymer interaction with the mean flow. As indicated in Fig. 3a, the Reynolds shear stress reduces with increasing drag reduction. For $DR = 60\%$ (L100W120LC), $-\overline{uv}^+$ is approximately a third of its magnitude in the Newtonian case. Conversely, the polymer stress increases with increasing drag reduction (Fig. 3b). At $DR = 60\%$, its near-wall contribution to Eq. (3.1) has the same magnitude as the Reynolds shear stress. In the case of the minimal channel,

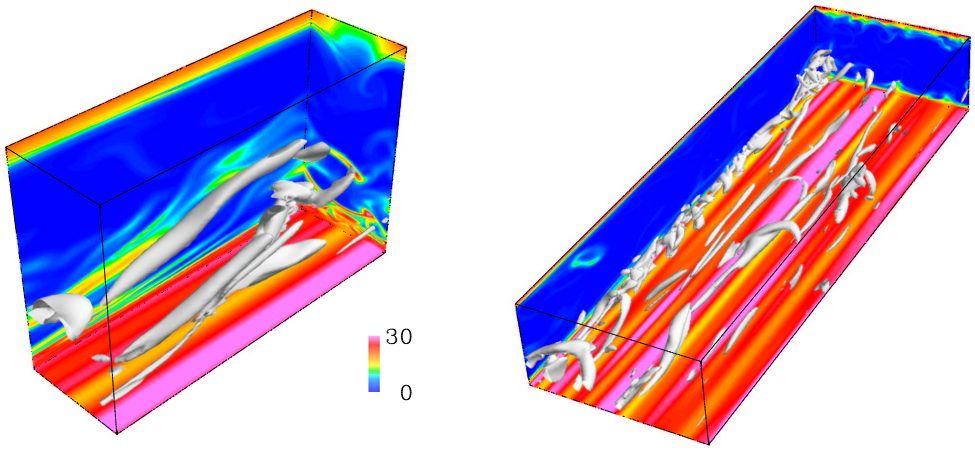

FIGURE 4. Snapshot of vortices identified by the Q-criterion (Dubief & Delcayre 2000) and the trace ($c_{kk}/L^2 \times 100$). *Left* L60W84MC; *right* L60W84LC. Vortices are only shown in the lower half of the domain.

the polymer stress is actually 1.5 higher than the Reynolds shear stress, which outlines the mechanism by which turbulence is sustained even in a minimal channel flow. The level of Reynolds shear stress and polymer stress are comparable to the ones measured by Ptasinski *et al.* (2001), even for their MDR experiment. Also plotted in Fig. 3b is the polymer stress contribution in case of zero-Reynolds shear stress as observed in the experiments of Warholic *et al.* (1999) and MDR, *i.e.* above $y^+ \sim 20$ the mean velocity profile is assumed to collapse with Virk's asymptotic profile (see Fig. 2a). In that case, the polymer stress is almost twice the one measured in the minimal channel flow for the same drag reduction. The different behavior observed in Ptasinski *et al.* (2001)'s experiment, as well as our simulation, and Warholic's demonstrates the essential role played by the polymer stress in the self-sustaining mechanism which produces the MDR turbulence.

4. Observations and perspectives on the drag reduction mechanism

The topology of the drag reduced flows is based on the same structures as Newtonian wall-turbulence: streaks and vortices. In Fig. 4, showing snapshots of L60W84MC and L60W84LC, the streaks are identified by the contours of the polymer extension c_{kk}/L^2 at the wall, where c_{kk} is the trace of c_{ij}. The regions of high and low stretch denotes high and low-speed streaks, respectively. The coherence of the streaks is rather impressive compared to Newtonian turbulence (not shown here). The streamwise persistence of the streaks has also been observed in White *et al.* (2003)'s experiments, as well as their spanwise stability. Vortices are identified using isosurfaces of the second invariant Q of the velocity gradient tensor. Positive values of $Q = \mathbf{\Omega}^2 - \mathbf{S}^2$, where $\Omega_{ij} = \partial_j u_i - \partial_i u_j$ and $S_{ij} = \partial_j u_i + \partial_i u_j$ isolate regions where the rotation rate dominates the strain rate, which provides a reliable identification method of vortices (Dubief & Delcayre 2000). The minimal channel flow contains a few, elongated vortices while the large domain has a more varied population of near-wall vortices, short and long quasi-streamwise vortices and hairpin-type vortices. These differences in the topology illustrate the different statistical behavior observed between the two simulation. On the side view, polymer extension is shown to burst away from the near-wall region intermittently in the upwash and downwash flows generated by vortices.

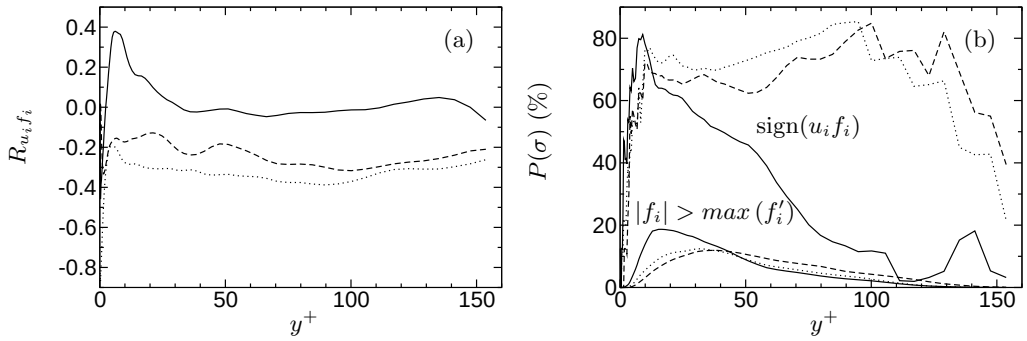

FIGURE 5. (a) Correlation velocity-viscoelastic stress in the three directions, ($R_{u_i f_i} = \overline{u_i f_i}/u_i' f_i'$, no summation on i). ——— , streamwise direction; - - - - , wall-normal; ····· , spanwise. (b) Conditional probabilities based on viscoelastic stress fluctuations satisfying $|f_i| < (\max(f_i'(y)), -h \le y \le +h)$ (the lower curves show the fraction of samples satisfying this condition). Upper curves: ——— , $P(uf_x > 0)$; - - - - , $P(vf_y < 0)$; ····· , $P(wf_z < 0)$. Data obtained from simulation L100W120MC.

The most interesting aspect of polymer drag reduction is to understand how such small concentrations of microscopic molecules can drive turbulence to states like the ones depicted in Fig. 4. One simple measure of the exchange of energy between the flow and polymers is the correlation velocity-viscoelastic stress,

$$\rho_i = \frac{\overline{u_i f_i}}{u_i' f_i'} \tag{4.1}$$

as shown in Fig. 5a (the viscoelastic stress f_i is defined in Eq. 2.1). The term $\overline{u_i f_i}$ enters the transport equation for the kinetic energy and through this term only the flow can be perturbed by polymers: when ρ_i is positive, polymers tend to enhance velocity fluctuations while $\rho_i < 0$, polymers dampen velocity fluctuations.

Only results from simulation L100W120MC are plotted since all simulations show the same trends. In the near-wall region, streamwise velocity fluctuations and viscoelastic stress fluctuations are positively correlated while, for the components normal to the mean flow, they are anti-correlated. Similar results were obtained by De Angelis *et al.* (2002) at LDR. The correlations indicates that the viscoelastic stress applies some opposition control on the transverse velocity fluctuations and plays a significant role in the increase of streamwise velocity fluctuations. Away from the viscous sublayer, the maximum correlation is about ± 0.3, ruling out the possibility that polymers enhance all streamwise velocity fluctuations nor oppose all the transverse ones.

Details of the viscoelastic stress action can only be captured by using conditional statistics. In this approach, we are interested in the large fluctuations of the viscoelastic stress, f_i since energy is exchanged between polymers and turbulence through this term. The probabilities $P((uf_x)(y) > 0, y \in [-h, +h])$, $P((vf_y) < 0, y \in [-h, +h])$ and $P((wf_z)(y) < 0, y \in [-h, +h])$ are computed over samples for which $|f_i|$ is larger than the maximum of the RMS f_i' over the entire channel. Also plotted are the fractions of samples satisfying such a condition for each component. The probability that $uf_x > 0$ peaks at 80% around $y^+ = 10$, while the probabilities that $vf_y > 0$ and $wf_z > 0$ exhibit a plateau in between 70% and 80% for $y^+ > 10$. These strong probabilities suggest that large fluctuations of viscoelastic stress are almost perfectly correlated to either turbulence enhancement for the streamwise component in the near wall region or to drag

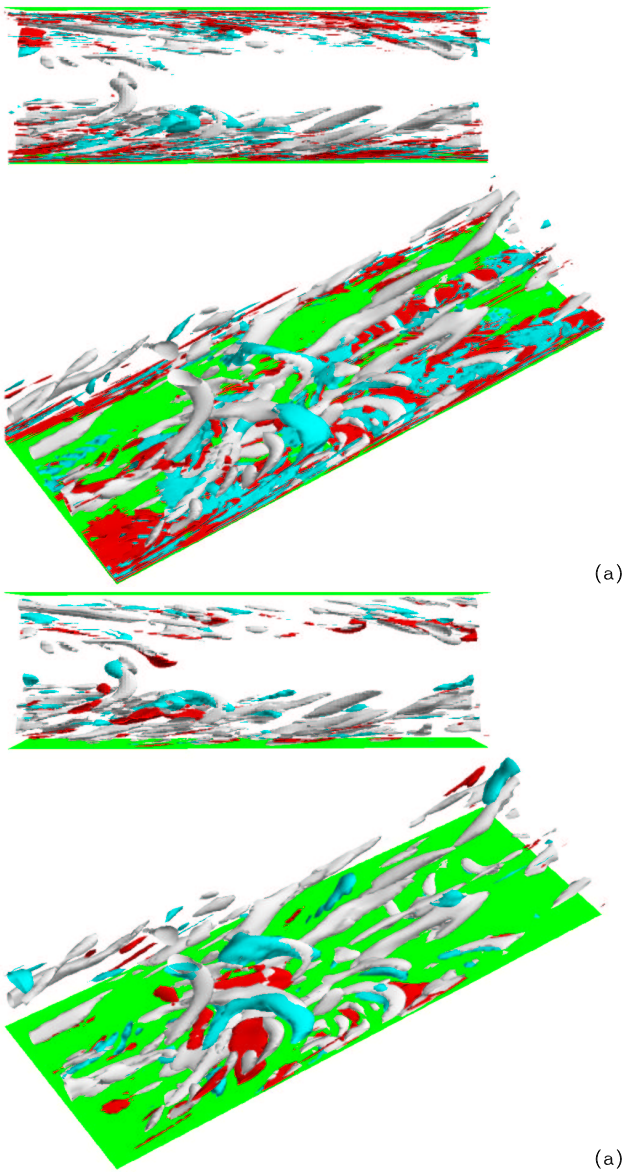

FIGURE 6. Snapshot of vortices (white isosurfaces) and isosurfaces of large viscoelastic stress fluctuations: blue, negative fluctuations; red, positive fluctuations. Fig. (a): streamwise viscoelastic stress; Fig. (b): wall-normal viscoelastic stress. The flow is from left to right, the bottom views show the lower half a portion of simulation L100W120LC, at $DR = 60\%$.

reduction for the transverse components in most of the channel. However it appears that large fluctuations of f_x away from the wall are highly anti-correlated with u fluctuations, indicating that where the mean shear is weak, f_x behaves like f_y or f_z. The separation of the drag reducing and drag enhancing activities between velocity components was also put forward by the numerical experiments (Dubief & Lele 2001) which isolated the action of polymers in the buffer region and also suggested that the drag reducing activ-

ity of the FENE-P equations comes predominantly from the wall-normal and spanwise components.

Fig. 6 illustrates the instantaneous location of large fluctuations of f_x and f_y. The view from the side gives an idea of the preferred location of these fluctuations while the view from the top indicates the relation between polymers and vortices. As observed in the correlation of u and f_x, a major portion of the large fluctuations is confined at the wall (Fig. 6a). Their occurrence is somewhat related with the presence of quasi-streamwise vortices in the buffer region and even above. The near-wall activity of the streamwise viscoelastic stress has just been shown (Fig. 5) to enhance streamwise velocity fluctuations however, away from the wall, the regions of large fluctuations are attached to the vortices in a similar way as the wall-normal viscoelastic stress (Fig. 6b). Large wall-normal viscoelastic stress appear to be produced exclusively around vortices and the same occurs for the spanwise fluctuations (not shown here). This observation holds regardless of the amount of DR. These visualizations show the strong correlation which exists between drag reducing polymer action and vortices.

5. Conclusion

A set of four viscoelastic simulations has been investigated, all in the high drag reduction regime, *i.e* change of slope in the log-law of the mean velocity profile and a significant decrease of Reynolds shear stress. Numerical experiment were performed in a minimal channel to show that the basic topology of drag reduced flow can be contained in a small computational domain. In its present form and for the polymer parameters under consideration, it appears that the FENE-P model does not produce enough stress to damp large scale structures in the outer region of the large domain. As drag reduction increases, the polymer stress is found to contribute as much as, and even in the minimal channel larger than, the Reynolds shear stress to the stress balance in the near-wall region. Therefore the polymer stress is essential for sustaining the weak turbulent state of MDR. The injection of energy from the polymers to the flow is confined to the very near wall region and it affects the streamwise velocity component only. Lastly, it is shown that the drag reducing activity targets exclusively the near-wall vortices, main source of turbulent friction drag (Kravchenko *et al.* 1993) and key ingredient of the autonomous regeneration cycle of near-wall turbulence (Jiménez & Pinelli 1999).

The support of DARPA and its project manager, Dr. Lisa Porter, are gratefully acknowledged. This work is sponsored by Defense Advanced Research Projects Agency, Advanced Technology Office, Friction Drag Reduction Program, DARPA order No.: K042/31, K042/13,N115/00. Issued by DARPA/CMO, Contract No.: MDA972-01-C-0041.

REFERENCES

De Angelis, E., Casciola, C. M. & Piva, R. 2002 DNS of wall turbulence: dilute polymers and self-sustaining mechanisms. *Comp. and Fluids* **31**, 495–507.

Dimitropoulos, C. D., Sureshkumar, R. & Beris, A. N. 1998 Direct numerical simulations of viscoelastic turbulent channel flow exhibiting drag reduction: Effect of variation rheological parameters. *J. Non-Newtonian Fluid Mech.* **79**, 433–468.

Dubief, Y. & Delcayre, F. 2000 On coherent-vortex identification in turbulence. *J. of Turbulence* **1** (011).

Dubief, Y. & Lele, S. K. 2001 Direct numerical simulation of polymer flow. In *Annual Research Briefs*, pp. 197–208. Center For Turbulence Research.

Dubief, Y., Terrapon, V. E., Shaqfeh, E. S. G., Lele, S. K. & Moin, P. 2003 The small-scale behavior of the FENE-P model in turbulent flow. *J. Comp. Phys.* To be submitted. extended version of: Dubief, Y. 2002 Direct numerical simulation of polymer flow. In *Annual Research Briefs*, pp. 197-208, Center For Turbulence Research.

Jiménez, J. & Moin, P. 1991 The minimal flow unit in near-wall turbulence. *J. Fluid Mech.* **225**, 213–240.

Jiménez, J. & Pinelli, A. 1999 The autonomous cycle of near-wall turbulence. *J. Fluid Mech.* **389**, 335–359.

Kravchenko, A. G., Choi, H. & Moin, P. 1993 On the relation of near-wall streamwise vortices to wall skin friction in turbulent boundary layers. *Phys. Fluids* **A 5** (12), 3307–3309.

Min, T., Yoo, J. Y. & Choi, H. 2001 Effect of spatial discretization schemes on numerical solutions of viscoelastic fluid flows. *J. Non-Newtonian Fluid Mech.* **100**, 27–47.

Ptasinski, P. K., Nieuwstadt, F. T. M., Van den Brule, B. H. A. A. & Hulsen, M. A. 2001 Experiments in turbulent pipe flow with polymer additives at maximum drag reduction. *Flow, Turbulence and Combustion* **66** (2), 159–182.

Sibilla, S. & Baron, A. 2002 Polymer stress statistics in the near-wall turbulent flow of a drag-reducing solution. *Phys. Fluids* **14** (3), 1123–1136.

Sureshkumar, R., Beris, A. N. & Handler, R. A. 1997 Direct numerical simulations of turbulent channel flow of a polymer solution. *Phys. Fluids* **9** (3), 743–755.

Terrapon, V. E., Dubief, Y., Moin, P. & Shaqfeh, E. S. G. 2003 Brownian dynamics simulation in a turbulent channel flow. In *2003 Joint ASME/JSME Fluids Engineeing Symposium on Friction Drag Reduction*. Honolulu, Hawaii, USA.

Virk, P. S. & Mickley, H. S. 1970 The ultimate asymptote and mean flow structures in Tom's phenomenon. *Trans. ASME E: J. Appl. Mech.* **37**, 488–493.

Warholic, M. D., Massah, H. & Hanratty, T. J. 1999 Influence of drag-reducing polymers on turbulence: effects of Reynolds number, concentration and mixing. *Exp. Fluids* **27**, 461–472.

White, C. M., Somandepalli, V. S. R. & Mungal, M. G. 2003 The turbulence structure of drag reduced boundary layer flow. *Exp. Fluids* To be published.